Rindler Modified Schwarzschild Geodesics

M. Halilsoy,[*] O. Gurtug,[†] and S. H. Mazharimousavi[‡]
Department of Physics, Eastern Mediterranean University,
G. Magusa, north Cyprus, Mersin 10, Turkey.

The mysterious attractive constant radial force acted in the past on Pioneer spacecrafts - the so-called Pioneer anomaly - is considered within the context of Rindler acceleration. As an idea this is tempting since it is reminiscent of the cosmological constant. Fortunately the anomalous force acts radially toward the sun so that it differs from the mission of a cosmological constant. Without resorting to the physical source responsible for such a term we investigate the modified Schwarzschild geodesics. The Rindler acceleration naturally affects all massive / massless particle orbits. Stable orbits may turn unstable and vice versa with a finely-tuned acceleration parameter. The overall role of the extra term, given its attractive feature is to provide confinement in the radial geodesics.

I. INTRODUCTION

In an attempt to describe gravity of a central mass at large distances and explain certain satellite anomalies Grumiller [1] gave a new metric in static spherically symmetric (SSS) spacetimes. The anomaly refers to the test particle behavior in the field of pairs, such as Sun-Pioneer spacecraft, Earth-satellites etc. and therefore it is of utmost importance [2]. The ansatz of SSS, naturally reduces the problem effectively to a two-dimensional system where the Newtonian central force modifies into $Force = -(\frac{M}{r^2} + a)$. Here M is the central gravitating mass while $a = const.$ is known as the Rindler acceleration parameter. For $a > 0$, the two forces are both toward center while $a < 0$, gives an outward repulsive force. Throughout our analysis in this paper we shall be using $a > 0$, unless stated otherwise. In particular, the attractive mysterious force acting on the Pioneer spacecrafts (10/11) launched in 1972 / 73 which could not be accounted by any known physical law came to be known as the Pioneer anomaly. We must add that a recent proposal based on thermal heat loss of the satellite may resolve the anomaly [3]. Among other proposals Modified Newtonian Dynamics (MOND) in the outer space attracted also interest. The fact that the Rindler force is a constant one dashes hopes to treat it as a perturbation due to other sources (or planets). Further, the non-isotropic role of parameter a differs it from the cosmological constant. Although it remains still open to investigate about the physical source that gives rise to such a term, herein we wish to study geodesics in the resulting spacetime. As a matter of fact in a separate study we have shown consistently that the Rindler acceleration parameter can be attributed to non-linear electrodynamics (NED) [4] ([4a]) and to a space-filling fluid in $f(R)$ gravity [4] ([4b]). In such a formalism the weak (and strong) energy conditions are satisfied. Such nice features, however, are not without pay off: global monopoles emerge as complementary objects to the energy conditions [4] ([4a]). For vanishing Rindler acceleration, $a = 0$, all results reduce to those of Schwarzschild as it should. Experimental estimates suggest that for the satellites $a \sim 10^{-10} m/s^2$, which suffices to yield significant differences at large distances. Let us add that in the vicinity of a Schwarzschild horizon $r = 2m$, any object feels a constant acceleration toward the black hole a lá Rindler. However, as stated above the Rindler acceleration in question refers to large distances and for this the central object need not be a black hole. In particular such a constant acceleration at certain distances from Earth (or any other planet) effects satellite motion to the extent that are dubbed as "anomalies". It should be, added that, in order that such 'anomalies' are universal each satellite / planet must feel it equally. So far no such anomaly is reported in objects other than the Pioneer spacecrafts.

The physical effects of the model proposed by Grumiller have been investigated in [5], by studying the classical solar system tests of general relativity. In that study, perihelion shifts, light bending and gravitational redshift were calculated for solar system planets in the presence of Rindler parameter. In another study [6], an alternative method has been employed to calculate the bending of light that affects the bounds on the Rindler parameter.

The main motivation of the present paper is to investigate the effect of the Rindler parameter a, on the trajectories of the timelike and null geodesics. Our analysis shows that the Rindler acceleration tends to confine the geodesics.

---

[*]Electronic address: mustafa.halilsoy@emu.edu.tr

[†]Electronic address: ozay.gurtug@emu.edu.tr

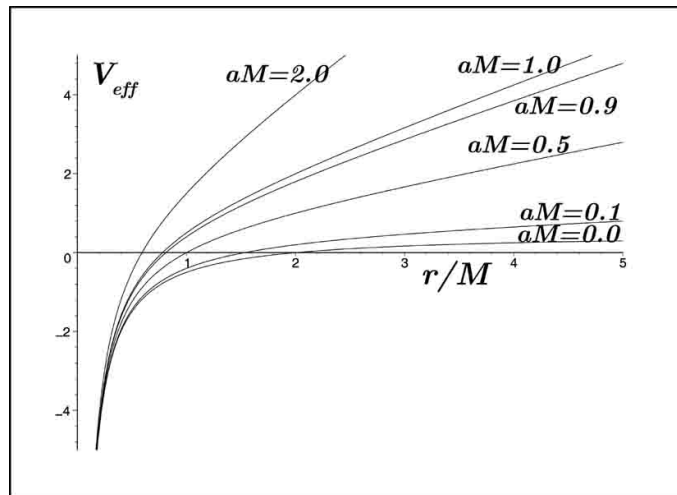[‡]Electronic address: habib.mazhari@emu.edu.tr

FIG. 1: *The effective potential V_{eff} (Eq. 26) rises with the increasing a. This behavior serves to confine geodesics nearer to the gravitating center.*

It would not be wrong to state that, with this remarkable property finely-tuned, Rindler parameter serves to have a kind of bounded cosmology.

No doubts the best account of Schwarzschild geodesics is given in "The Mathematical Theory of Black Holes" by Chandrasekhar [7]. Being integrable systems the geodesic equations do not exhibit chaotic behavior. It is known that in some gravitational systems such as Kundt Type-III and type-N spacetimes chaos is indispensable [8] (and references cited therein). The Rindler modified Schwarzschild spacetime on the other hand is a type-D spacetime.

In this paper, we follow a similar procedure as was done for Schwarzschild metric [7]. To be more precise, we will closely follow the method used in [9]. The motivation behind this is to compare the effect of Rindler parameter that deviates the results from the analysis performed in [7]. The paper is organized as follows. The review of Grumiller's spacetime and its type-D character is emphasized in section II. In section III, the derivation of the particles trajectorie for timelike and null geodesics with their numerical plots are presented. Null geodesics in terms of elliptic functions are given in the Appendix. Our Conclusion is given in section IV.

II. STRUCTURE OF GRUMILLER'S SPACETIME

Grumiller have proposed a model for gravity at large distances of a central object by assuming static and spherically symmetric system. The corresponding line element in the absence of cosmological constant is given by

$$ds^2 = -f\left(r\right)dt^2 + \frac{dr^2}{f\left(r\right)} + r^2\left(d\theta^2 + \sin^2\theta d\phi^2\right), \tag{1}$$

where

$$f\left(r\right) = 1 - \frac{2M}{r} + 2ar. \tag{2}$$

Herein M is the mass of the central object (or black hole) and $a \geq 0$ is a real constant. With $a = 0$, Eq. (1) reduces to the Schwarzschild black hole. The only horizon of the metric is given by $f\left(r\right) = 0$ which yields

$$r_h = \frac{-1 + \sqrt{1 + 16Ma}}{4a}. \tag{3}$$

It can easily be checked that for $a \to 0$, we obtain $r_h = 2M$, as it should be. Furthermore the scalars of the spacetime are given by

$$R = -12\frac{a}{r}, \tag{4}$$

$$R_{\mu\nu}R^{\mu\nu} = 40\frac{a^2}{r^2}, \tag{5}$$

$$K = R_{\mu\nu\alpha\beta}R^{\mu\nu\alpha\beta} = 48\frac{M^2}{r^6} + 32\frac{a^2}{r^2} \tag{6}$$
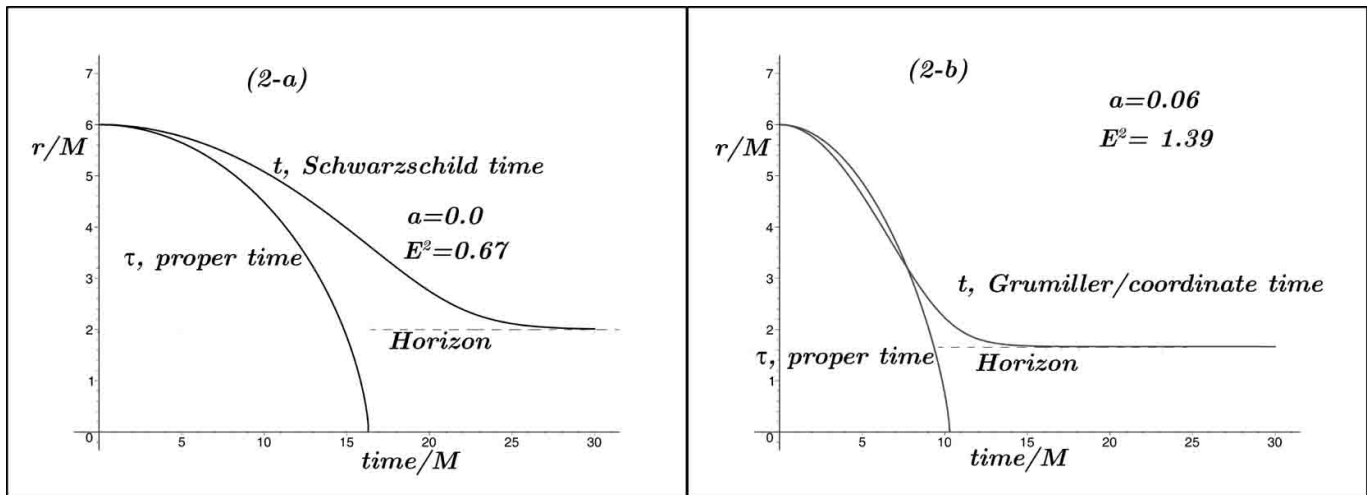
FIG. 2: *Particle-fall into $r = 0$ singularity versus times (i.e. coordinate and proper) in (a) Schwarzschild and (b) Grumiller metric. Outside the horizon criss-crossing of geodesics in (b) differs from the Schwarzschild case. The fall evidently delays in (a) compared to (b).*

which indicate the typical central curvature singularity at $r = 0$ behind the event horizon.

A. The Description of the Grumiller Spacetime in a Newman-Penrose (NP) Formalism

The Grumiller's metric is investigated with the Newman-Penrose (NP) formalism [10] in order to explore the physical properties of the metric or clarifying the role of Rindler parameter on the physical quantities. Note that the signature of the metric given in (1) is changed in this section to $(+, -, -, -)$, apt for the NP formalism. The set of proper null tetrad $1-$forms is given by

$$l = dt - \frac{dr}{f(r)},$$ (7)

$$n = \frac{1}{2}\left(f(r)dt + dr\right),$$

$$m = -\frac{r}{\sqrt{2}}\left(d\theta + i\sin\theta d\varphi\right),$$

and the complex conjugate of m. The non-zero spin coefficients in this tetrad are

$$\beta = -\alpha = \frac{\cot\theta}{2\sqrt{2}r}, \quad \rho = -\frac{1}{r}, \quad \mu = -\frac{f(r)}{2r}, \quad \gamma = \frac{1}{4}\frac{df(r)}{dr}.$$ (8)

We obtain as a result, the Weyl and Ricci scalars as

$$\Psi_2 = -\frac{M}{r^3},$$ (9)

$$\phi_{11} = \Lambda = -\frac{a}{2r},$$

so that the spacetime is Petrov type-D. The Rindler acceleration parameter is seen to effect only the Ricci components, leaving the mass term Ψ_2 of Schwarzschild unchanged. In the so called Pioneer anomaly the attractive force suggests that $a > 0$, which is the case that we shall investigate in this paper. However, the fact that $\phi_{11} < 0$, under the choice $a > 0$ which violates the energy conditions suggests also that the underlying physical source is not a familiar one. In a separate study [4], we showed explicitly what the physical source may be, and we reached the conclusion that the arrow indicates an unaccustomed source: the non-linear electrodynamics (NED). Pure electric/magnetic sources with unusual Lagrangian of NED does yield the Rindler-type acceleration term without violating the energy conditions. We restate that, in this paper, we shall investigate only the resulting geodesics without touching the possible physical source of the Rindler parameter a.
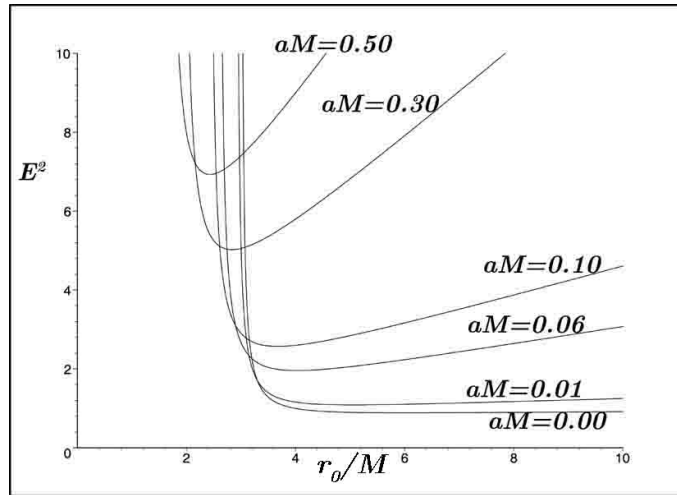
FIG. 3: A plot of E^2 versus r_0/M (Eq. (32)) of a massive particle starting at rest from r_0, moving along a timelike geodesic for various values of aM.

III. PARTICLE TRAJECTORIES

The Lagrangian for a massive particle with unit mass is given by

$$\mathcal{L} = \frac{1}{2}g_{\mu\nu}\dot{x}^\mu\dot{x}^\nu = -\frac{1}{2}f(r)\dot{t}^2 + \frac{\dot{r}^2}{2f(r)} + \frac{1}{2}r^2\left(\dot{\theta}^2 + \sin^2\theta\dot{\phi}^2\right) \tag{10}$$

in which a dot "·" shows derivative with respect to an arbitrary parameter σ. There are two conserved quantities, the energy E and the angular momentum ℓ in ϕ direction,

$$E = \frac{\partial\mathcal{L}}{\partial\dot{t}} = g_{tt}\frac{dt}{d\sigma} = -f(r)\frac{dt}{d\sigma} = \text{constant} \tag{11}$$

and

$$\frac{\partial\mathcal{L}}{\partial\dot{\phi}} = r^2\sin^2\theta\dot{\phi} = \ell = \text{constant}. \tag{12}$$

Note that $\ell = r^2\dot{\phi}$ is the angular momentum of the particle moving on the plane $\theta = \frac{\pi}{2}$. For null ($\epsilon = 0$) and timelike ($\epsilon = 1$) geodesics one has,

$$g_{\mu\nu}\frac{dx^\mu}{d\sigma}\frac{dx^\nu}{d\sigma} = -\epsilon \tag{13}$$

which on the plane of motion $\theta = \frac{\pi}{2}$ implies

$$\left(\frac{dr}{d\sigma}\right)^2 = E^2 - f(r)\left(\epsilon + \frac{\ell^2}{r^2}\right). \tag{14}$$

This equation can be cast into a familiar form of equation of motion for a unit mass test particle

$$\frac{1}{2}\left(\frac{dr}{d\sigma}\right)^2 + V_{eff}(r) = \mathcal{E}_{eff} \tag{15}$$

with an effective potential $V_{eff}(r) = \frac{1}{2}f(r)\left(\epsilon + \frac{\ell^2}{r^2}\right)$ and corresponding effective energy $\mathcal{E}_{eff} = \frac{1}{2}E^2$. The exact form of the effective potential can be written as

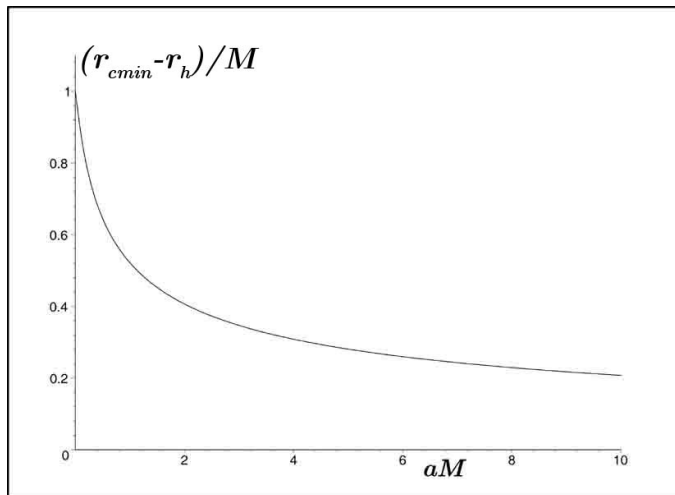$$V_{eff}(r) = \frac{1}{2}\left(1 - \frac{2M}{r} + 2ar\right)\left(\epsilon + \frac{\ell^2}{r^2}\right). \tag{16}$$

FIG. 4: *The difference between circular geodesics radii ($r_{c\,\min}$) and horizon radii (r_h) is shown as a function of aM. For increasing aM it shows that the circular geodesics approach to the horizon.*

We note that the classical region which r may take is limited by the constraint $\mathcal{E}_{eff} \geq V_{eff}(r)$ to keep r real. Using the chain rule $\frac{dr}{d\sigma} = \frac{dr}{d\phi}\frac{\ell}{r^2}$, one finds

$$\left(\frac{dr}{d\phi}\right)^2 = \frac{2r^4}{\ell^2}\left(\mathcal{E}_{eff} - V_{eff}(r)\right). \tag{17}$$

As in the standard Kepler problem for convenience, we introduce $r = \frac{1}{u}$ which yields the $u-$equation for future use

$$\left(\frac{du}{d\phi}\right)^2 = \frac{E^2}{\ell^2} - \left(1 - 2Mu + \frac{2a}{u}\right)\left(\frac{\epsilon}{\ell^2} + u^2\right). \tag{18}$$

In the sequel we shall use this general equation to investigate the motion of the particle in different cases.

A.   Motion with zero angular momentum: radial

In zero angular momentum case (i.e. $\ell = 0$) the motion will remain in the plane $\phi =$constant and the particle will move radially. This in turn implies from (14) that

$$\left(\frac{dr}{d\sigma}\right)^2 = E^2 - \epsilon f(r). \tag{19}$$

In the following subsections we shall study the cases $\epsilon = 0$ (null) and $\epsilon = 1$ (timelike) separately. First, let's consider the null geodesics (i.e., $\epsilon = 0$):

1.   Null geodesics $\epsilon = 0$

In null geodesics, which refers to the motion of a massless particle (photon), Eq. (19) becomes

$$\left(\frac{dr}{d\sigma}\right)^2 = E^2. \tag{20}$$

We recall from (11) that $E = -f(r)\frac{dt}{d\sigma}$ and therefore after some modification this equation becomes

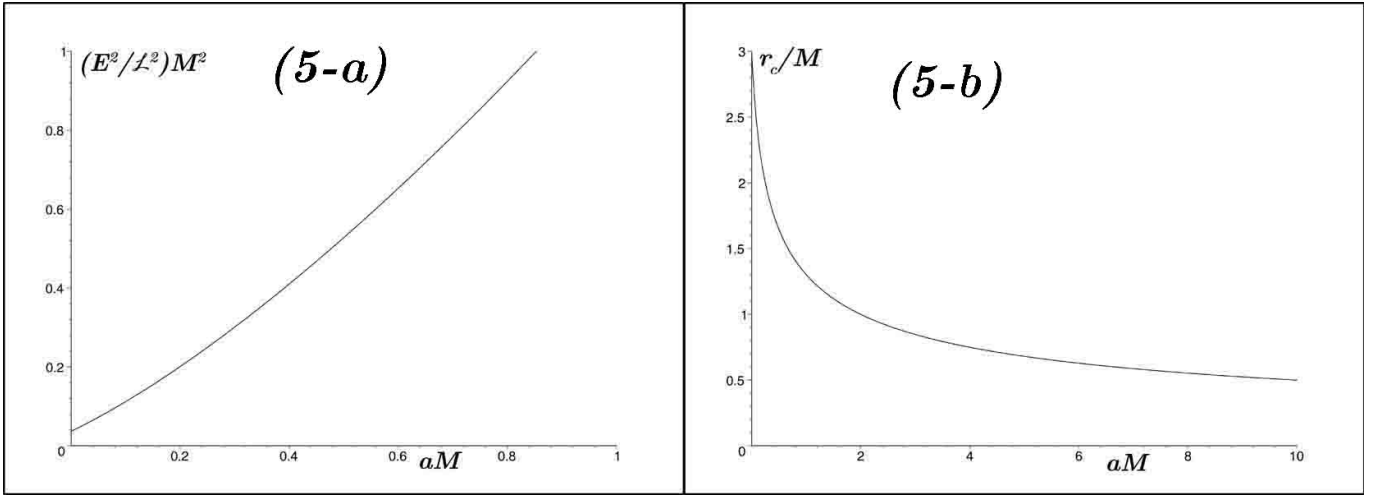$$\frac{dr}{dt} = \pm f(r) = \pm\left(1 - \frac{2M}{r} + 2ar\right), \tag{21}$$

FIG. 5: Plot of $\left(\frac{E^2}{\ell^2}\right)M^2$ and $\frac{r_c}{M}$ (Eq. (41) and (40)) in terms of aM for a massless particle. These figures show that for larger a (with a given mass M) the circular orbit of the photon has smaller radius but larger value of $\left(\frac{E^2}{\ell^2}\right)$.
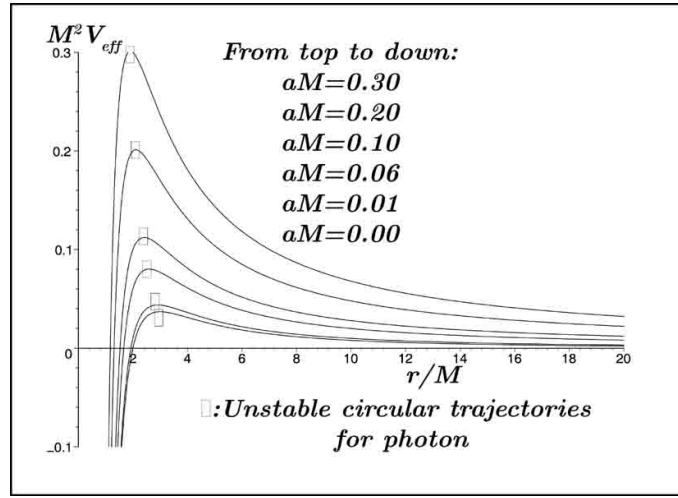

FIG. 6: The $M^2 V_{eff}$ plot versus $\frac{r}{M}$ for photons shows the unstable circular orbits for photons. In this range of aM no stable photon orbits exist.

which explicitly admits the following integral between the time and the radial position of the photon,

$$\frac{\ln\left(\frac{r-2M+2ar^2}{r_0-2M+2ar_0^2}\right)}{4a} + \frac{\left[\tanh^{-1}\left(\frac{1+4ar}{\sqrt{16Ma+1}}\right) - \tanh^{-1}\left(\frac{1+4ar_0}{\sqrt{16Ma+1}}\right)\right]}{2a\sqrt{16Ma+1}} = \pm(t-t_0). \tag{22}$$

Herein r_0 is the initial position of the massless particle (photon) and t is the time measured by the distant observer while t_0 is the initial time.

2. Timelike Geodesics $\epsilon = 1$

In the case of timelike geodesics (i.e., $\epsilon = 1$), which refers to the motion of a massive particle, with unit mass Eq. (19) becomes

$$\left(\frac{dr}{d\sigma}\right)^2 = E^2 - 1 + \frac{2M}{r} - 2ar, \tag{23}$$

which can be cast into the following equation of motion

$$\frac{d^2r}{d\sigma^2} = -\frac{M}{r^2} - a. \tag{24}$$

Choosing σ to be the proper time, τ, one finds

$$\frac{d^2r}{d\tau^2} = -\left(\frac{M}{r^2} + a\right). \tag{25}$$

Considering $a > 0$, clearly the radial force per unit mass is attractive and toward the central object / black hole. Now let's consider the particle initially at rest and, upon the gravitational attraction, starts moving from its initial radial location $r = r_0$. Using (23) with $\sigma = \tau$ one finds

$$E^2 = 1 - \frac{2M}{r_0} + 2ar_0 \tag{26}$$

and therefore

$$\left(\frac{dr}{d\tau}\right)^2 = 2a\left(r_0 - r\right) + 2M\left(\frac{1}{r} - \frac{1}{r_0}\right). \tag{27}$$

Further, the effective potential in radial motion reads

$$V_{eff}(r) = \frac{1}{2}\left(1 - \frac{2M}{r} + 2ar\right) \tag{28}$$

and upon introducing $\frac{r}{M} = \tilde{r}$, $Ma = \tilde{a}$ we find $V_{eff}(\tilde{r}) = \frac{1}{2}\left(1 - \frac{2}{\tilde{r}} + 2\tilde{a}\tilde{r}\right)$, which is depicted in Fig. 1. In this figure the horizon $\tilde{r}_h$ is the intersection of $V_{eff}(\tilde{r})$ with $\tilde{r}$ axis. This figure shows that with the Rindler parameter there is an upper bound for the motion of the particle. Hence, unlike the Schwarzschild spacetime with $\mathcal{E}_{eff} \geq 1$(for $a = 0$ /Schwarzschild spacetime, there is an upper bound for the motion of the particle if $\mathcal{E}_{eff} \leq 1$.), the particle can not escape to infinity. Finally, using Eq.s (23) and (11) one finds

$$\left(\frac{dr}{dt}\right)^2 = \frac{1}{E^2}\left(E^2 - 1 + \frac{2M}{r} - 2ar\right)\left(1 - \frac{2M}{r} + 2ar\right)^2 \tag{29}$$

which after differentiating with respect to t one obtains,

$$\frac{d^2r}{dt^2} = -\frac{12}{E^2 r^4}\left(M + ar^2\right)\left(M - ar^2 - \frac{r}{2}\right)\left(M + \left(\frac{E^2}{3} - \frac{1}{2}\right)r - ar^2\right). \tag{30}$$

Here also t is the time measured by the distant observer. In Fig.s 2a and 2b we plot the variation of the coordinate time (t) and the proper time (τ) along a timelike radial-geodesic described by the test particle, starting at rest at $r = r_0$ and falling towards the singularity. We comment that the conserved energy of the particle is found from Eq. (29), i.e.

$$0 = \frac{1}{E^2}\left(E^2 - 1 + \frac{2M}{r_0} - 2ar_0\right)\left(1 - \frac{2M}{r_0} + 2ar_0\right)^2 \tag{31}$$

and consequently

$$E^2 = 1 - \frac{2M}{r_0} + 2ar_0. \tag{32}$$

From Fig.s 2a and 2b, it is observed that the Rindler parameter accelerates the particles following the timelike geodesics so that the particles reach the singularity faster than the Schwarzschild case. In Fig. 3 we plot E^2 versus $\frac{r_0}{M}$ for different values of aM. This figure clearly shows that for non-zero a, energy possesses a minimum value.
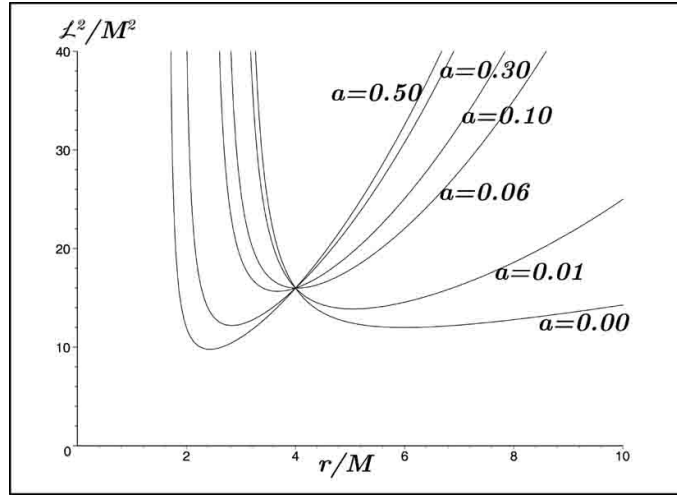
FIG. 7: *Angular momentum behavior of a massive particle versus distance for changing a (Eq. (43)). It is observed that all curves coincide at $\frac{r}{M} = 4$.*

B.   Circular Motion

After considering the radial motion, in this section we study the circular motion of a photon and a test massive particle by considering $\frac{du}{d\phi}\big|_{u=u_c} = 0$ (Eq. (18)) in which $r_c = 1/u_c$ is the circular orbit of the particle. This condition, in turn implies

$$\frac{E^2}{\ell^2} - \left(1 - 2Mu_c + \frac{2a}{u_c}\right)\left(\frac{\epsilon}{\ell^2} + u_c^2\right) = 0. \tag{33}$$

Once more let's look at Eq. (18) and find derivative of both sides with respect to φ which gives

$$\frac{d^2u}{d\phi^2} = \frac{d}{du}\left(\frac{E^2}{\ell^2} - \left(1 - 2Mu + \frac{2a}{u}\right)\left(\frac{\epsilon}{\ell^2} + u^2\right)\right).$$

In order to have equilibrium motion $\frac{d^2u}{d\phi^2} = 0$ must hold and this in turn implies

$$\frac{d}{du}\left[\frac{E^2}{\ell^2} - \left(1 - 2Mu + \frac{2a}{u}\right)\left(\frac{\epsilon}{\ell^2} + u^2\right)\right]\Bigg|_{u=u_c} = 0. \tag{34}$$

These conditions yield the expressions for the angular momentum ℓ and the energy E of the particle as

$$\ell^2 = \frac{\epsilon\left(Mu_c^2 + a\right)}{u_c^2\left(a + u_c - 3Mu_c^2\right)}, \tag{35}$$

$$E^2 = \frac{4\epsilon\left(a + \frac{u_c}{2} - Mu_c^2\right)^2}{u\left(a + u_c - 3Mu_c^2\right)}. \tag{36}$$

We note that the considered spacetime is nonasymptotically flat. Hence, the value of r_c is bounded. For a physically acceptable motion the constraint $a + u_c - 3Mu_c^2 > 0$ arises naturally from Eq. (35) which in turn admits $r_c > \frac{-1+\sqrt{1+12Ma}}{2a} = r_{c\,\text{min}}$. Here $r_{c\,\text{min}}$ is clearly larger than the horizon $r_h = \frac{-1+\sqrt{1+16Ma}}{4a}$ so that $r_{c\,\text{min}} - r_h = \frac{2\sqrt{1+12Ma}-\sqrt{1+16Ma}-1}{4a} > 0$. In Fig. 4 we plot $\frac{r_c - r_h}{M}$ in terms of Ma which implies that with larger a, although the gap between $r_{c\,\text{min}}$ and r_h gets smaller, it always remains positive. Note that to have a physical orbit $r_c > r_h$ must hold.
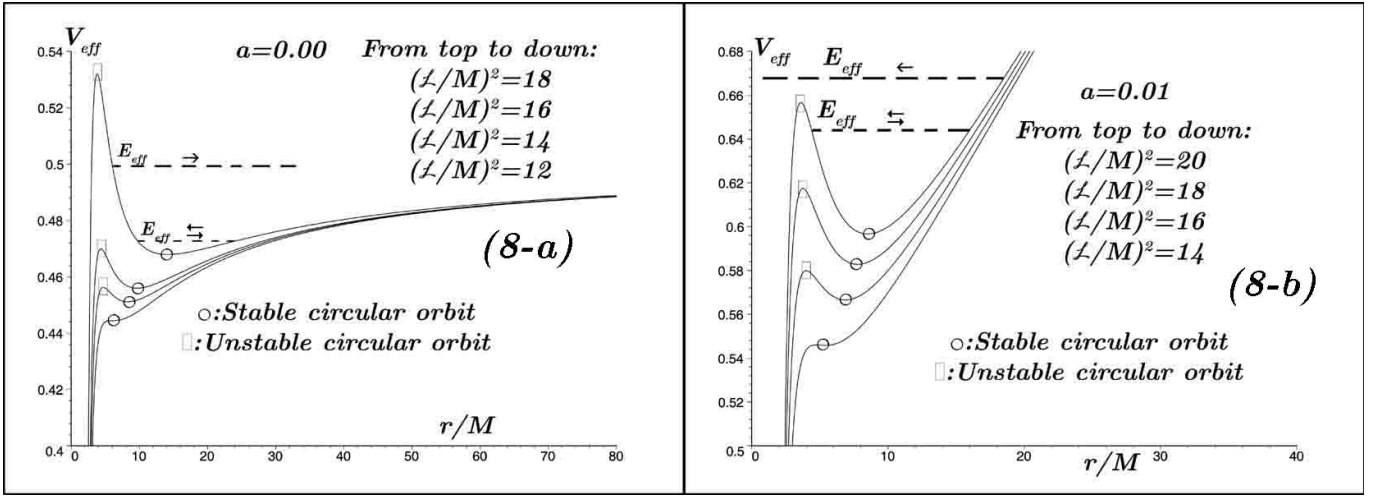
FIG. 8: V_{eff} for massive particles versus $\frac{r}{M}$ for (a) the Schwarzschild case ($a = 0$) and (b) the Grumiller case with $a = 0.01$ and various values of $\frac{E^2}{\ell^2}$. The potential barriers are comparatively shown in both cases. The steeply rising potential barrier in (8b) explains why the orbits remain bounded. This doesn't occur in (8a). The minimum stable orbit can be obtained from $\left.\frac{dV_{eff}}{dr}\right|_{r=r_{\min}} = 0$ and $\left.\frac{d^2 V_{eff}}{dr^2}\right|_{r=r_{\min}} = 0$, which yields the Rindler parameter a in terms of $r_{\min}$ as $a = \frac{\ell^2}{r_{\min}^3}\left(\frac{3M}{r_{\min}} - \frac{1}{2}\right)$.

1. Null geodesics ($\epsilon = 0$)

In the case of null geodesics we set $\epsilon = 0$ in Eq.s (33) and (34) to obtain

$$r_c = \frac{-1 + \sqrt{1 + 12aM}}{2a} \tag{37}$$

and

$$\frac{E^2}{\ell^2} = \frac{\left(1 + \sqrt{1 + 12aM} + 24aM\right)\left(1 + \sqrt{1 + 12aM}\right)}{108M^2}. \tag{38}$$

Having r_c known an exact value for the specific M and a means that for the photon there exist only one equilibrium circular orbit with the ratio $\frac{E^2}{\ell^2}$ given in the latter equation. In Fig. 5 we plot $\frac{E^2 M^2}{\ell^2}$ and $\frac{r_c}{M}$ versus aM. It shows that for larger a (with a given mass M) the circular orbit of the photon has larger value of $\left(\frac{E^2}{\ell^2}\right)$ and smaller value of r_c.

To complete present analysis we study the stability of such orbits. This can be done by considering the geodesic equation of the photon in Eq. (14) with $\epsilon = 0$ which becomes

$$\frac{1}{\ell^2}\left(\frac{dr}{d\sigma}\right)^2 + \frac{f(r)}{r^2} = \frac{E^2}{\ell^2}. \tag{39}$$

A replacement of $\sigma = \frac{\tilde{\sigma}}{\ell}$ gives

$$\left(\frac{dr}{d\tilde{\sigma}}\right)^2 + V_{eff} = E_{eff} \tag{40}$$

in which

$$V_{eff} = \frac{f(r)}{r^2} = \frac{1 - \frac{2M}{r} + 2ar}{r^2} \tag{41}$$

and

$$E_{eff} = \frac{E^2}{\ell^2}. \tag{42}$$

To have a stable circular orbit we must have $\left.V_{eff}'\right|_{r_c} = 0$ and $\left.V_{eff}''\right|_{r_c} > 0$. We have plotted V_{eff} in Fig. 6, showing that, there is no stable circular orbit for photons. As a remark to this section let us add that in case that the source of the Rindler acceleration is NED [5] the null geodesics do not represent in general the photon orbits.
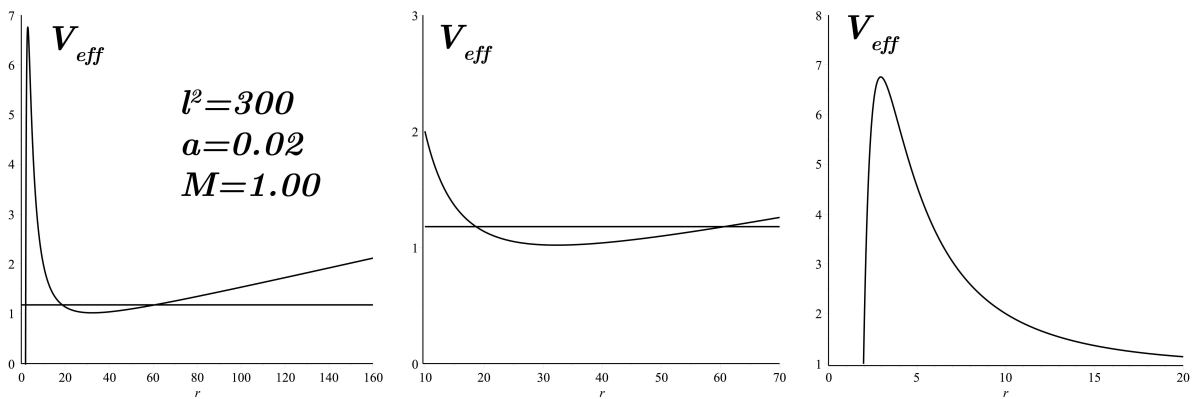
FIG. 9: V_{eff} for massive particles versus r as a particular example for $M = 1$, $a = 0.01$ and $\ell^2 = 300$. The inscriptions depict enlarged form of unstable and stable parts. The horizontal line shows two turning points.

2. Time-like geodesic $\epsilon = 1$

A similar argument is valid also for a massive particle. We set $\epsilon = 1$ in Eq.s (35) and (36) to get

$$\ell^2 = \frac{\left(Mu_c^2 + a\right)}{u_c^2 \left(a + u_c - 3Mu_c^2\right)} \tag{43}$$

and

$$E^2 = \frac{4\left(a + \frac{u_c}{2} - Mu_c^2\right)^2}{u_c \left(a + u_c - 3Mu_c^2\right)}. \tag{44}$$

As we mentioned before here $r_c = \frac{1}{u_c}$ is the radius of the equilibrium circular orbit. Fig. 7 shows the variation of ℓ^2/M^2 versus r/M (Eq. (43)) in terms of a which clearly shows that once $r \to r_c$ the angular momentum goes to infinity. In the case of ℓ^2, as one can see from Eq. (43) and Fig. 7, $\frac{r}{M} = 4$ is the only orbit in which irrespective to the value of a, $\frac{\ell^2}{M^2} = 16$.

To investigate the stability of the equilibrium circular motion of a massive particle we consider the effective potential of the dynamic motion of the particle given in (16). Again in a stable circular motion the requirements are $V'_{eff}\big|_{r_c} = 0$ and $V''_{eff}\big|_{r_c} > 0$.

Figures 8a and 8b display the effective potential in terms of r/M for $a = 0.00$ and $a = 0.01$ respectively. We see almost similar behavior but still in the presence of a the stable orbits occur with larger ℓ (for a given mass). The most important difference between the two curves occurs in the behavior of the graphs to the right of the minimum points. As it is seen in Fig. 8a, the graph eventually is concave down and becomes asymptotically constant while in Figure 8b it is concave up and steeply rising. These indicate that (8b) is different from the $a = 0$ case where for a given energy larger than the asymptotic value of V_{eff} particle would escape to infinity. In the presence of a, particles can't escape to infinity. Even if the energy is bigger than the local maximum, to the left of the minimum, the particle would fall into the singularity of the spacetime.

In Fig. 9 we plot V_{eff} in terms of r for $M = 1$, $a = 0.01$ and a particular value for $\ell^2 = 300$. The minimum and maximum of the potential are highlighted. Fig. 10a shows the circular orbit of a massive particle with unit mass at $r_c = r_{\min}$. An infinitesimal deviation from $r_{\min}$ yields a particle orbit falling into the singularity (Fig. 10b). In Fig. 11a the stable circular orbit at $r_c = r_{\max}$ is shown explicitly while in Fig. 11b the perturbed orbits confined around $r_{\max}$ is depicted.

IV. CONCLUSION

In this paper, the geodesic analysis of the Grumiller's metric which describes gravity at large distances is considered. The effect of the Rindler parameter is investigated and compared with the Schwarzschild geodesics. Timelike and null geodesics are obtained numerically both for radial and circular motion. Exact radial solutions also are available
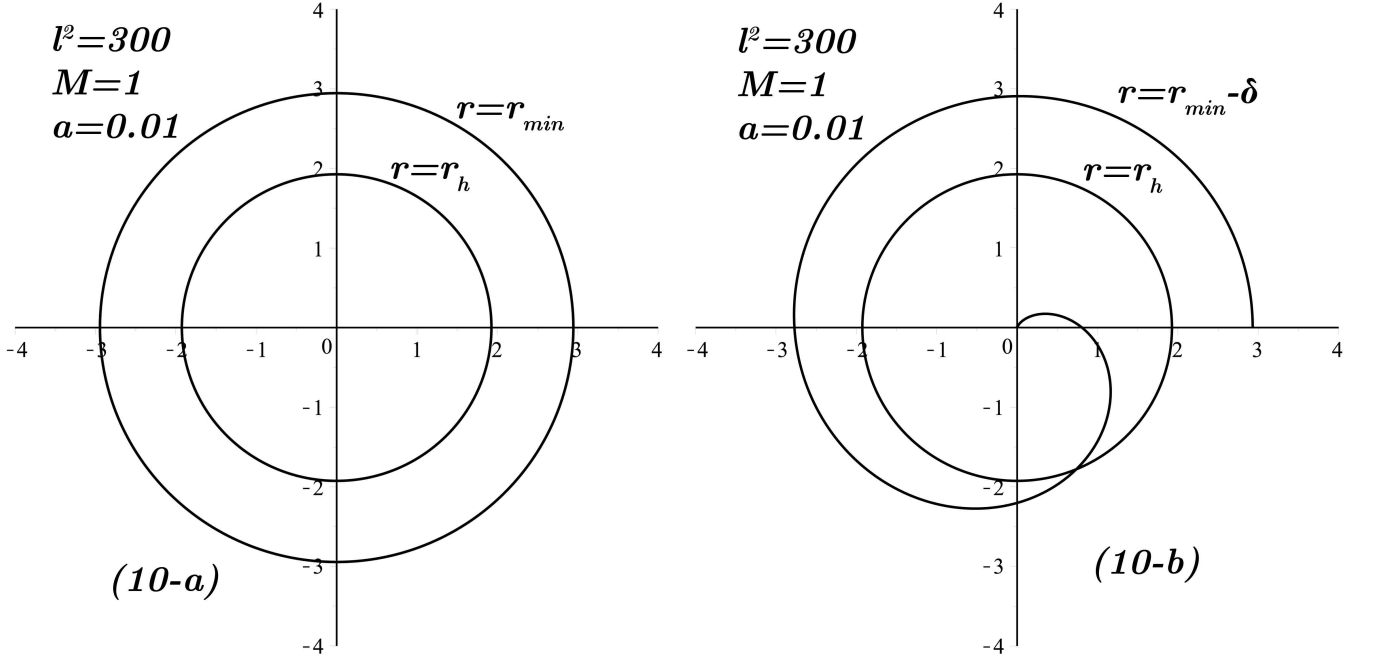
FIG. 10: a. Details of the circular orbits from Eq. (18), ($\frac{dr}{d\phi} = 0$). From $E^2 = 13.51647495 = (1 - \frac{2}{r} + 2.02r)\left(1 + \frac{300}{r^2}\right)$ the minimum circular radius becomes $r_c = r_{min} = 2.944698040$ whereas the horizon radius is $r_h = 1.925824025$. b. A small perturbation of r_{min} in 10a by $r_0 = r_{min} - \delta$ where δ is a small positive number ($\delta \ll 1$) causes the geodesics to plunge into the singularity. This is the fate of the unstable orbits. The differential equation is solved by "A seventh-eighth order continuous Runge-Kutta method (dverk78)" method and then the results have been ploted. The tolerances for the absolute and relative local error are chosen to be 10^{-8}.
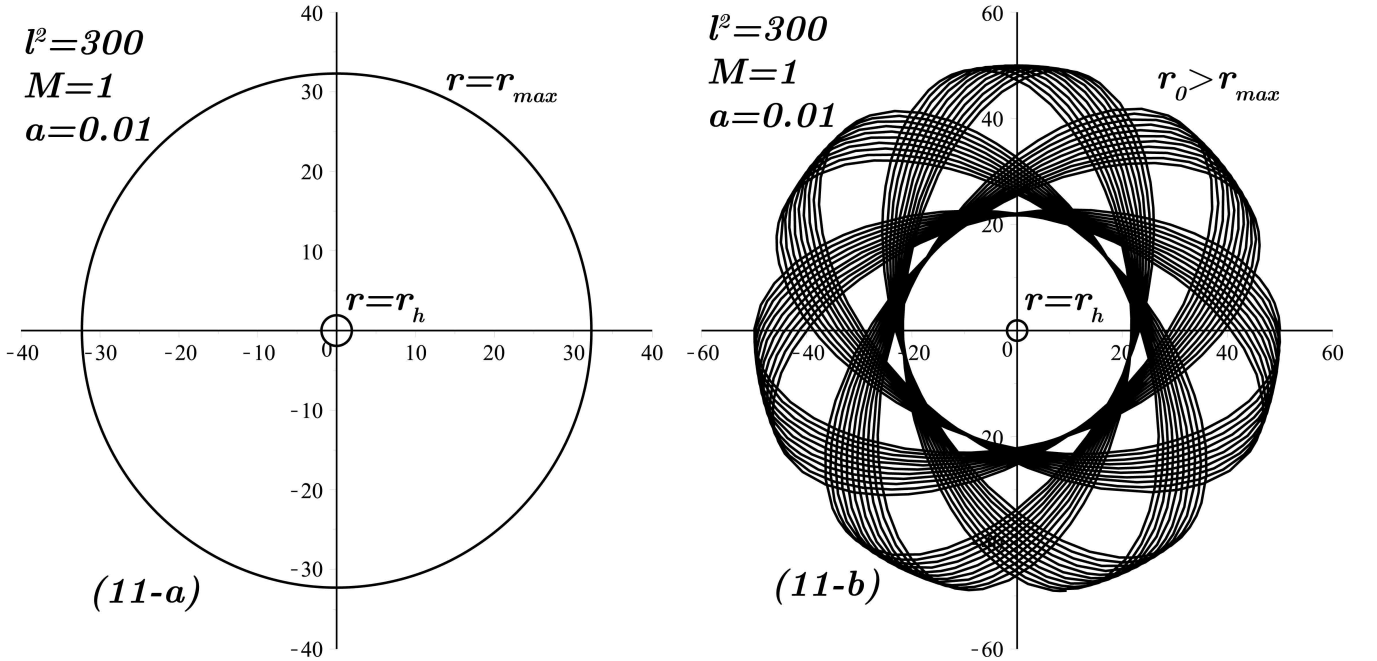

FIG. 11: The circular orbits displaying r_{max} at the minimum for the V_{eff} in Fig. 9. Any distortion of the particle around r_{max} in 11-a gives the closed pattern around r_{max} so that the particle becomes confined between two radii. Recall that r_0 is the initial radial position of the particle in the potential well. The differential equation is solved by "A seventh-eighth order continuous Runge-Kutta method (dverk78)" method and then the results have been ploted. The tolerances for the absolute and relative local error are chosen to be 10^{-8}.
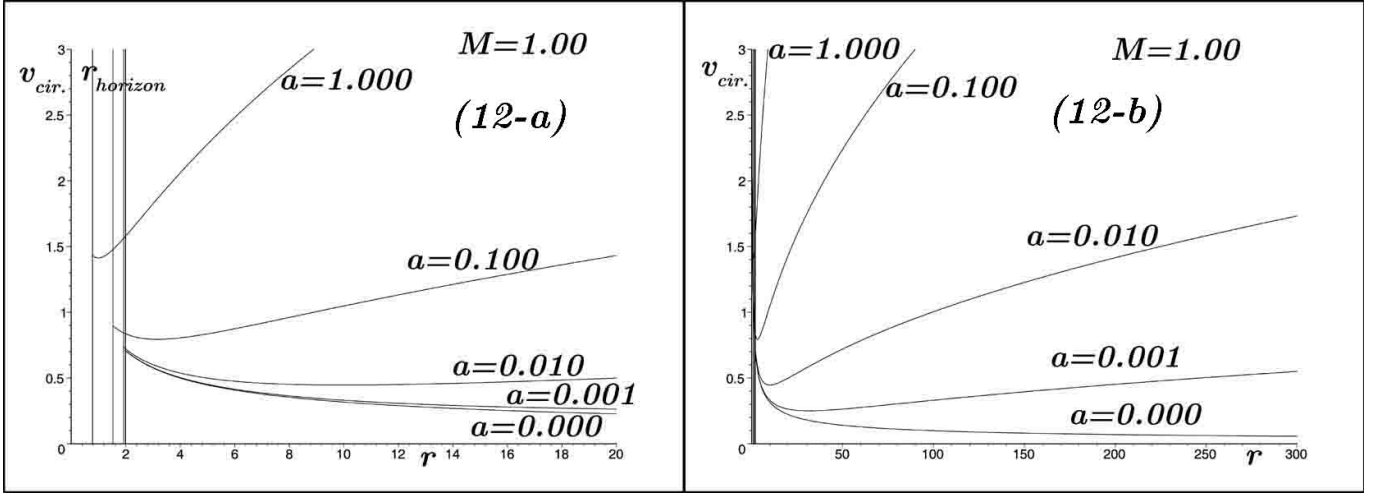
FIG. 12: Circular velocity plots versus radial distances, at small (a) and large (b) scales. It is observed that in order to obtain flat rotation curves i.e. horizontal line $v(r)$ for circular velocity versus distance the Rindler acceleration parameter must be rather small (i.e. $a \ll 1$). At the smaller scale (a) the horizon (r_h) is also shown.
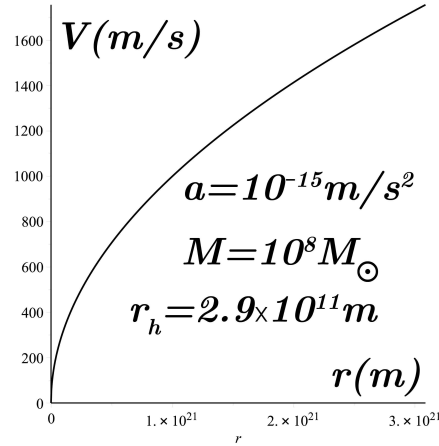

FIG. 13: Circular velocity plots versus radial distances r for a realistic value of $a = 10^{-15} m/s^2$. The value of M is taken from [1] for a dwarf galaxies i.e., $M = 10^8 M_\odot$. As it is observed the effect of Rindler acceleration is strong for $r > 10^{20} m$.

for null geodesics as shown in the Appendix. Since our choice is $a > 0$, this amounts to the confinement of geodesics around the central object outside the event horizon. Closed periodic orbits bounded between two radii are depicted in Fig. (11b).

For the radial motion; the motion of the particle is bounded with the inclusion of the Rindler parameter. Hence, unlike the Schwarzschild case, the particle can not escape to infinity. This is not unexpected since both mass and Rindler terms are attractive. Plunging into the central singularity from unstable geodesics due to small perturbation is favored by virtue of the Rindler acceleration term.

In conclusion, without identifying its physical origin the extra term $\sim 2ar$ in the spherical geometry adds much novelties and richness to the Schwarzschild geodesics. Given the astrophysical distances in spite of the small $a \sim 10^{-12} m/s^2$, the Rindler term $\sim 2ar$ becomes still significant. By adjusting a small Rindler parameter flat rotation curves can be obtained as depicted in Fig. 12. We recall that the velocity $v(r)$ (with unit mass) is given from the relation $|Force| = \frac{M}{r^2} + a = \frac{v^2}{r}$ [1].

Appendix: Exact Elliptic Solution to the null Geodesic Equations

Let's consider the Lagrangian for variable θ :

$$\mathcal{L} = -\frac{1}{2}f\left(r\right)\left(\frac{dt}{d\lambda}\right)^2 + \frac{1}{2f\left(r\right)}\left(\frac{dr}{d\lambda}\right)^2 + \frac{1}{2}r^2\left(\frac{d\theta}{d\lambda}\right)^2 + \frac{1}{2}r^2\sin^2\theta\left(\frac{d\varphi}{d\lambda}\right)^2 \tag{A.1}$$

where λ is the affine parameter. Employing the Mino time [11] γ which is defined as $d\lambda = r^2 d\gamma$ for convenience it becomes

$$\mathcal{L} = -\frac{1}{2}\frac{f\left(r\right)}{r^4}\left(\frac{dt}{d\gamma}\right)^2 + \frac{1}{2r^4 f\left(r\right)}\left(\frac{dr}{d\gamma}\right)^2 + \frac{1}{2r^2}\left(\frac{d\theta}{d\gamma}\right)^2 + \frac{1}{2r^2}\sin^2\theta\left(\frac{d\varphi}{d\gamma}\right)^2 \tag{A.2}$$

which together with the metric condition

$$-\frac{f\left(r\right)}{r^4}\left(\frac{dt}{d\gamma}\right)^2 + \frac{1}{r^4 f\left(r\right)}\left(\frac{dr}{d\gamma}\right)^2 + \frac{1}{r^2}\left(\frac{d\theta}{d\gamma}\right)^2 + \frac{1}{r^2}\sin^2\theta\left(\frac{d\varphi}{d\gamma}\right)^2 = \epsilon \tag{A.3}$$

yield the geodesics equations as:

$$\frac{dt}{d\gamma} = \frac{r^3}{\Delta}\alpha \tag{A.4}$$

$$\frac{d\varphi}{d\gamma} = \frac{\beta}{\sin^2\theta} \tag{A.5}$$

$$\left(\frac{d\theta}{d\gamma}\right)^2 = k - \frac{\beta^2}{\sin^2\theta} \tag{A.6}$$

and

$$\left(\frac{dr}{d\gamma}\right)^2 = \left(\epsilon r^2 - k\right)r\Delta + r^4\alpha^2. \tag{A.7}$$

1. The r-equation

In these equations k, α and β are integration constants and $\Delta = rf\left(r\right) = r - 2M + 2ar^2$. Following the method introduced in [12] r-equation (A7), after introducing $r = \pm\frac{1}{x} + r_0$ in which r_0 is a root for $\left(\epsilon r^2 - k\right)r\Delta + r^4\alpha^2 = 0$ and setting $\epsilon = 0$ becomes

$$\left(\frac{dx}{d\gamma}\right)^2 = b_0 + b_1 x + b_2 x^2 + b_3 x^3 \tag{A.8}$$

in which

$$b_0 = \alpha^2 \tag{A.9}$$

$$b_1 = \pm\frac{2r_0\alpha^2\left(2r_0 - 4M + 3ar_0^2\right)}{r_0 - 2M + 2ar_0^2}$$

$$b_2 = \frac{r_0^2\alpha^2\left(5r_0 - 12M + 6ar_0^2\right)}{r_0 - 2M + 2ar_0^2}$$

$$b_3 = \pm\frac{2r_0^3\alpha^2\left(r_0 - 3M + ar_0^2\right)}{r_0 - 2M + 2ar_0^2}.$$

Finally a further transformation

$$x = \frac{4y - \frac{b_2}{3}}{b_3} \tag{A.10}$$

eliminates the second order and (A8) reads

$$\left(\frac{dy}{d\gamma}\right)^2 = 4y^3 - g_2 y - g_3 \tag{A.11}$$

where

$$g_2 = \frac{b_2^2 - 3b_1 b_3}{12} \tag{A.12}$$

and

$$g_3 = \frac{b_1 b_2 b_3}{48} - \frac{b_2^3}{216} - \frac{b_0 b_3^2}{16}. \tag{A.13}$$

The final form of the equation (A11) is nothing but of elliptic type and its solution is the WeierstrassP function [13] i.e,

$$y(\gamma) = WeierstrassP(\gamma - \gamma_0, g_2, g_3) \tag{A.14}$$

where γ_0 is an integration constant. One obtains as a result

$$r = \pm \frac{b_3}{4 WeierstrassP(\gamma - \gamma_0, g_2, g_3) - \frac{b_2}{3}} + r_0. \tag{A.15}$$

Let us note that for $\epsilon = 1$ i.e. for time like geodesics, the foregoing method does not work, at least the solution is not in elliptic form. For this reason we considered the null geodesics alone.

2. θ and φ-equations

θ-equation (A6) can be easily solved and the analytic answer is given by

$$\theta_\pm(\gamma) = \pi \pm \cos^{-1}\left(\sqrt{\beta}(\gamma - \tilde{\gamma}_0)\right) \tag{A.16}$$

in which $\tilde{\gamma}_0$ is an integration constant. After θ one can integrate the φ-equation to find

$$\varphi(\gamma) = \sqrt{\beta}\left(\sqrt{\beta}(\gamma - \tilde{\gamma}_0)\right) + \varphi_0 \tag{A.17}$$

in which φ_0 is an integration constant.

[1] D. Grumiller, Phys. Rev. Lett. **105**, 211303 (2010) [Erratum-ibid. **106**, 039901 (2011)];
D. Grumiller and F. Preis, Int. J. Mod. Phys. D **20**, 2761 (2011).
[2] J. D. Anderson, P. A. Laing, E. L. Lau, A. S. Liu, M. M. Nieto and S. G. Turyshev, Phys. Rev. Lett. **81**, 2858 (1998).
[3] S. G. Turyshev, V. T. Toth, G. Kinsella, S. C. Lee, S. M. Lok and J. Ellis, Phys. Rev. Lett. **108**, 241101 (2012).
[4] M. Halilsoy, O. Gurtug and S. H. Mazharimousavi, arXiv:1212.2159;
S. H. Mazharimousavi and M. Halilsoy, Mod. Phys. Lett. A, **28**, 1350073 (2013).
[5] S. Carloni, D. Grumiller and F. Preis, Phys. Rev. D **83**, 124024, (2011).
[6] J. Sultana and D. Kazanas, Phys. Rev. D **85**, 081502(R), (2012).
[7] S. Chandrasekhar, *The Mathematical Theory of Black Holes*, Clarendon Press, Oxford (2004).
[8] J. Podolsky and K. Vesely, Phys. Rev. D **58**, 081501 (1998);
I. Sakalli and M. Halilsoy, Phys. Rev. D **74**, 067501 (2006);
I. Sakalli and M. Halilsoy, Chin. Phys. Lett. **28**, 070402 (2011).
[9] S. Guha, P. Bhattacharya and S. Chakraborty, Astrophys Space Sci **341**, 445 (2012);
E. Hackmann and C. Lämmerzahl, Phys. Rev. Lett. **100**, 171101 (2008a);
E. Hackmann and C. Lämmerzahl, Phys. Rev. D **78**, 024035 (2008b);
E. Hackmann, V. Kagramanova, J. Kunz and C. Lämmerzahl, Phys. Rev. D **78**, 124018 (2008);
N. Cruz, M. Olivares and J. R. Villanueva, Class. Quantum Gravity **22**, 1167 (2005);
J.-P. Uzan and R. Lehoucq, Eur. J. Phys. **22**, 371 (2001);
F. Dahia, C. Romero, L. F. P da Silva and R. Tavakol, J. Math. Phys. **48**, 072501 (2007);
F. Dahia, C. Romero, L. F. P da Silva and R. Tavakol, Gen. Relativ. Gravit. **40**, 1341 (2008).

[10] E. Newman and R. Penrose J. Math. Phys. **3**, 566 (1962).

[11] Y. Mino, Phys. Rev. D **67**, 084027 (2003).

[12] V. Kagramanova, J. Kunz, E. Hackmann and C. Lammerzahl, Phys. Rev. D. **81**, 124044 (2010);
S. Grunau and V. Kagramanova, Phys. Rev. D **83**, 044009 (2011).

[13] A. I. Markushevich, Theory Of Functions of a Complex Variable (Prentice-Hall, Englewood Cliffs, NJ, 1967), Vol. III.